HHS Public Access

Author manuscript

Ophthalmology. Author manuscript; available in PMC 2021 February 08.

Published in final edited form as:

Ophthalmology. 2018 June ; 125(6): 929–937. doi:10.1016/j.ophtha.2017.12.006.

Gaze evoked deformations in optic nerve head drusen: repetitive shearing as a potential factor in the visual and vascular complications

Patrick A Sibony, MD[1], **Junchao Wei, PhD**[1], **Ian A. Sigal, PhD**[2,3]

[1]Department of Ophthalmology, SUNY Stony Brook, Stony Brook, NY

[2-]Department of Ophthalmology, University of Pittsburgh, Pittsburgh, PA

[3]McGowan Institute For Regenerative Medicine, University of Pittsburgh, Pittsburgh, PA

Abstract

Objective: To determine if ocular ductions deform intrapapillary and peripapillary tissues in optic nerve head drusen(ONHD) and compare these deformations to normals and other optic neuropathies.

Design: Observational case series.

Participants: 20 patients with optic nerve head drusen

Methods: Axial rasters of the optic nerve from a spectral-domain optical coherence tomography(SD-OCT) [Cirrus 5000. Zeiss Meditch] were used to analyze the shape of the peripapillary basement membrane-layer (ppBM-layer) in 20 confirmed cases of ONHD. We compared registered images obtained two eye positions: 10-15° in adduction and 30-40° degrees in abduction. Geometric Morphometrics was used to analyze the shape of the ppBM-layer defined by placing 10 equidistant landmarks extending 2500 microns on both sides of the basement membrane opening. We also adapted an image strain tracking technique to measure regional intrapapillary strains in six of our patients. Using manually placed “nodes” on the reference image (in adduction), an iterative, block-matching algorithm is used to determine local displacements between the reference and its paired image in abduction. Displacement vectors were used to calculate the mean shear and effective strain(%change)

Main Outcome Measures: Peripapillary shape deformations, intrapapillary shear strains and effective strains

Results: We found a statistically significant difference in the shape of the ppBM-layer between abduction and adduction(p=0.01). The deformation was characterized by a relative posterior displacement temporally in adduction that reversed in abduction. Strain tracking in all six patients showed substantial gaze-induced shearing and effective strains. Mean effective strains were 7.5%

Corresponding author: Patrick A Sibony, MD, Department of Ophthalamology, University Hospital and Medical Center, Health Sciences Center, SUNY Stony Brook, NY 11794.

No conflicts

outside the drusen. Shear and effective strains were significantly larger outside than within the drusen ($p<0.003$ and <0.01, respectively).

Conclusions: The clinical importance of gaze-induced deformations is unknown but this study suggests that repetitive gaze-induced shearing may be a factor in the evolution and complications of ONHD. Shearing strains are often more damaging to neural tissue than compressive or tensile strains. ONHD are byproducts of degenerating axons. ONHD appear to be a consequence of two parallel pathways: 1.an ill-defined neurodegenerative axonopathy that initiates the process and 2.a cycle of mechanically-mediated axonal injury that progressively forms new calcific deposits, enlarges existing drusen, injures adjacent axons and damages blood vessels.

Optic nerve head drusen (**ONHD**) are intrapapillary calcifications that range in size between 5-1000 microns.. Early on, buried deep within the prelaminar optic nerve head (**ONH**), they may not be seen ophthalmoscopically; but will gradually become visible as they enlarge and approach the surface. The associated elevation and blurring of the disc can be confused with papilledema. ONHD are associated with a slowly progressive loss of peripheral vision and rarely, acute vision loss from neuro-retinal vascular complications.[1–5] The root cause of ONHD and its complications are unknown.

Using spectral domain optical coherence tomography (**SD-OCT**), we and others have recently shown that horizontal ocular ductions induce deformations of the ONH and peripapillary tissues in normal subjects, [6–8] anterior ischemic optic neuropathy (**AION**) and papilledema.[6] These studies led us to consider whether stress and strain on the ONH induced by ocular ductions may be a factor in the progressive loss of visual field and vascular complications of ONHD. Our goal was: (i) to determine if ocular ductions deform intrapapillary and peripapillary tissues in patients ONHD using shape analysis and strain tracking techniques; (ii) to compare these deformations to previously published data in normals and other optic neuropathies and (iii) to consider the role gaze-evoked strains in the evolution and complications of ONHD.

METHODS and Materials

Inclusion criteria

The diagnosis of optic nerve head drusen was based on the typical ophthalmoscopic features that included visible intrapapillary refractile deposits, sometimes associated with elevation of the optic disc, vascular anomalies, and peripapillary retinal pigment epithelial changes. Irrespective of whether drusen were visible or buried, all patients had a B scan or fundus autofluorescence photographs that confirmed the diagnosis. All patients had OCT findings consistent with the diagnostic criteria defined by the Optic Disc Drusen Studies Consortium Recommendations[9] for the diagnosis. We excluded any patient with coexistent disc anomaly (e.g. tilted optic disc, high myopia, staphylomas, or otherwise dysplastic), optic neuropathies or papilledema.

Image Acquisition

A Cirrus 5000 SD-OCT (Carl Zeiss Meditec, Inc. Dublin, CA) was used to acquire a (1) 200x200 optic disc cube and (2) a 5-line, high definition, axial raster (9mm in length 0.125

mm intervals) with a signal strength of ≥ 7. The optic disc cube was used to calculate the mean RNFL thickness. The Cirrus 5000 SD-OCT produces vertically stretched raster images with an aspect ratio of 3:2 (750 x 500 pixels [px]) (figure 1). We corrected the aspect ratio from 3:2 to an unstretched aspect ratio of 9:2 (750 x 167 px) for shape analysis. To illustrate small differences, some of the figures are displayed in a stretched or 3:2 aspect ratio where indicated.

High definition 5 line axial rasters were obtained in two head positions with the eyes in adduction and abduction to the extent that the patient and device would permit. Adduction was limited by the patient's nose against the lens element of the device at approximately 10-15° and abduction was less restricted at approximately 30-40°. These ranges were based on rotational head positions while the patient viewed the OCT fixation target using a head mounted protractor. Scanning laser ophthalmoscopic image stabilization ("FastTrac",) was used to register images. We used the most centrally positioned raster of the 5 raster lines in adduction as a baseline reference to compare to the axial raster obtained in abduction at the same location ("Tracked to Prior" option). Images were mirrored horizontally when necessary to align the temporal and nasal regions.

Geometric Morphometric Shape Analysis

We employed Geometric Morphometrics (GM) to analyze the shape of the ppBM-layer imaged on the SD-OCT raster. This is a well-established method that quantifies and analyzes shape and its covariation with other variables. [10–13] The methodologies are detailed in a primer by Zelditch et al.[13] Additional references and software can be found online at http://life.bio.sunysb.edu/morph. [12] The application of this technique to the analysis of the ONH has been described in several previous publications.[6, 14–16] The "tps" software [12] was used in this analysis. A brief description follows.

GM defines shape as that geometric property that remains after normalizing for differences in centroid location, scale and rotation.

Digitizing semi-landmarks: Using, imaging software (Photoshop; Adobe Systems, San Jose, CA) we superimposed a 2500μ rectilinear grid on the temporal and nasal side of the basement membrane opening (BMO) of a 9mm axial raster image (unstretched (9:2) aspect ratio) The grid was used to position 10 equidistant "semi-landmarks" (defined as landmarks placed along a curve or surface) spanning a distance of 2500 μm from the edge of the basement membrane-layer (ppBM-layer) on both sides of the BMO. Each semi-landmark was positioned along the outer edge of the ppBM-layer starting at the edge of the BMO. [Figure 1a]. Semi-landmark placement was performed on image files that were de-identified with respect to name and eye position.

Generalized Procrustes Analysis or Procrustes superimposition is the process of superimposing all of the specimen shapes onto a mean shape in three sequential steps: first by translating the centroid of the semi-landmarks to single point of origin; then rescaling to a uniform size and finally minimizing rotational differences between corresponding landmarks.

The thin plate spline displays differences in shape as a smooth deformation, using an algorithm that interpolates differences between landmarks and can be visualized using vectors at each landmark. The thin plate spline also defines a set of shape variables (partial warps) that capture the differences between shapes. The partial warp scores generate data matrices that can be analyzed with the proper degrees of freedom using multivariate statistical methods

Principal Component Analysis (PCA) is used to identify and ordinate the variation in shape along a series of components that are linear combinations of the partial warps. In effect, PCA identifies the important patterns of shape based on variance to determine if they distinguish patient groups (in this case shape differences between abduction and adduction). The relative contribution of each principal component is expressed as a percent of the total variance. Principal Component Analysis was performed using a variance - covariance matrix of the shape variables.

Statistical Analysis of Shape is based on comparing the sums of squared Procrustes differences between and within the samples expressed as an F-ratio. The evaluation compares the observed F-value to a distribution based on 10,000 random permutations of the individuals to the groups being compared. The proportion of Goodall's F statistics from these permutations equal to or larger than the observed Goodall's statistic is interpreted as the "p value" for the test. In order to avoid correlation bias between eyes within an individual, all statistical analyses on shape were performed on the right eye or in unilateral cases the affected eye. A Students t test was used to compare the means of continuous variables. Analysis of variance (ANOVA) was used to complete multiple comparisons of continuous variables.

Strain tracking

We adapted recently developed image tracking techniques, to measure local deformations (strains) between abduction and adduction in six of our cases where intrapapillary image quality permitted. The methods are detailed elsewhere. [17–19] Briefly, the source image in abduction, was brought into rough registration with the target image (in adduction), using a rigid body transformation. Next, a set of discrete landmarks were manually placed on the target, to use as reference locations for registration between the images. An iterative, block-matching algorithm minimizing the zeroed normalized cross-correlation function was then applied to determine the local displacement vectors that bring a block surrounding the landmarks of interest from the source into optimal coincidence with the target. The image matching was then refined using a subpixel phase correlation based on paired image subregions. From the resulting discrete vector field, the full field displacement and strain tensor were computed and interpolated.

Tissues can be stretched, compressed or sheared, sometimes simultaneously, in various directions. For simplicity, we focused on "shear strains" and "effective shear strains". Shear strains were chosen because they are a major factor in neural tissue damage.[20, 21] Effective strains are convenient because they summarize the multidimensional state of strain into a single value, taking into account tension, compression and shear.[8] Effective strains are also helpful to compare with previous ONH tracking studies.[8] Effective strains were computed

using the methodology of Wang et al. [8] For analysis, images were “unstretched” by expanding them laterally by a factor of 3. For presentation, they were “stretched” again by the reverse process.[22] For each subject, two regions of interest were manually defined, one within the drusen and another outside. The mean shear and effective strains within the regions were computed and compared via paired t-test.

This study was approved and complies with policies of the SUNY Stony Brook Committee on Research Involving Humans and complied with Declaration of Helsinki.

RESULTS

We identified 20 patients with ONHD. There were 16 females and 6 males with a mean age of 32 ± 15 (range 16-55). Fourteen of the patients had ONHD bilaterally and 6 were unilateral. ONHD were visible in 15 of the cases and buried in 5.

Figure 1b shows a scatter plot of normalized landmarks after Procrustes superimposition from each subject in abduction(red circle) and adduction (black circle). The continuous lines show the mean (consensus) shapes in abduction(black) and adduction (red). Because the differences were small, the image is stretched vertically three fold (figure 1c) to illustrate the change in more detail. Relative to abduction, the shape in adduction is displaced posteriorly on the temporal side of the BMO relative to the nasal side. The pattern in abduction is reversed. The difference in the mean shape between abduction and adduction was statistically significant to a level of $p < 0.01$ (permutation)

To characterize those features that best distinguish the shape differences in eye position we performed a Principal Component Analysis on a variance - covariance matrix of the shape variables derived from the semi-landmark data (figure 2). The first three principal components accounted for 90% of the variance in shape. PC1, accounting for 70% of the variance, implied a shape characterized by an anterior (toward vitreous) - posterior (away from vitreous) axial displacement of the ppBM-layer. PC2, accounted for 12% of the variance, captured differences in the diameter of the basement membrane opening. PC3 accounted for 8% of the variance was characterized by a seesaw tilting with posterior displacement temporally and slight anterior displacement nasally on the positive side of the ordinate. The reverse pattern was depicted on the negative side of the ordinate.

PC3 was the one component that most clearly distinguished the shapes associated with abduction and adduction. Although there was considerable overlap in shapes across subjects, paired comparisons of each subject showed a consistent pattern where all but 3 of the patients displayed a positive shift along the ordinate when going from abduction to adduction. Said differently, most patients in abduction had a relative anterior displacement temporally (toward the vitreous, relative negative position on the ordinate) that on adduction shifted posteriorly (away from the vitreous, positively along the ordinate). A symmetrical relative posterior shift in adduction was also seen in PC1. There was no clear distinction between abduction and adduction with respect to PC2.

An example of an axial raster from one of the subjects showing a slight relative posterior displacement temporally is shown in figure 3. A video clip from another subject is shown online (figure 4).

We did not find any correlation between shape or change in shape (deformation) with the mean RNFL, the size or visibility of the druse.

Strain tracking revealed that the change in gaze caused substantial intrapapillary tissue deformations in all six cases studied, as shown in figure 5. Deformations outside the drusen were significantly larger than within. Shear strains were, on average, 7.6 times larger outside the drusen than within (3.8% vs. 0.5%, $p<0.003$). Effective strains were, on average, 3.4 times larger outside the drusen than within (7.2% vs. 2.1%, $p<0.01$).

DISCUSSION.

This study shows that patients with ONHD display significant gaze-evoked deformations in the shape of the ppBM-layer and substantial strains within the prelaminar ONH surrounding ONHD.

Deformation of the ppBM-layer, in adduction, consists of a relative posterior displacement temporally relative to the nasal side. The pattern is reversed in abduction. The difference in the overall shape between adduction and abduction was statistically significant ($p < 0.01$, permutation). The shape pattern that best distinguished the effects of ocular ductions was most evident in the third principle component (PC3) which implies a seesaw type of deformation. Demer [23] has proposed that gaze-evoked deformations in normals are caused by the optic nerve sheath tethering the globe especially in adduction. It is likely that optic nerve sheath tethering also explains the deformations in ONHD.

To compare the shape changes in ONHD to normals and other optic neuropathies, we reanalyzed a previously published GM shape analysis [6] on normals, AION and papilledema and combined them with the patients from this study with ONHD. The methodology for both acquisition and analysis using GM was identical in both studies. We found that the patterns and magnitudes of the deformations in ONHD (figure 6) showed no significant difference (ANOVA) between AION, normals and drusen; all three however were significantly different from papilledema where gaze induced deformations were greatly exaggerated in the latter.

Strain tracking in all six patients studied showed substantial gaze induced shearing and effective strains (figure 5). Shear and effective strains were significantly larger outside than within the drusen ($p<0.003$ and <0.01, respectively). Mean effective strains were 7.5% outside the drusen, larger than the 5.8% reported by Wang et al. as induced within the lamina cribrosa of healthy subjects.[8] In one individual, shear deformations outside the drusen were more than 18 times larger than within. In the same individual, effective strains outside the drusen reached 14.8%.

The functional impact of ocular ductions on the normal ONH is unknown. It is likely that ocular ductions induce multiple modes of stress and strain (i.e. effective strains) that arise

from (i) a seesaw shearing within the ONH (ii) tensile extension of the sheath and optic nerve [23] and (iii) kinking of the optic nerve at the scleral opening. [24] These empirical observations are consistent with finite element analyses showing alternating gaze induced strains in the peripapillary sclera; temporally in adduction and nasally in abduction. [24, 25] The transient dynamic effects of ocular ductions may also affect the type and magnitude of strains possibly greater than the static deformations might otherwise indicate. [6, 26] The pattern of shape deformation and the strain tracking observed in this study as well as others previously reported in normals suggest that ocular ductions generates a shearing strain within the ONH. [6–8, 24, 25]

Although the peripapillary and intrapapillary strains of ONHD (and normals) are relatively small, their impact may be affected by the way in which intrapapillary calcifications change the material properties, structural geometry and stress/strain distribution within the ONH. Fluid Structure Interaction models have shown that repetitive pulsatile loads (from blood flow) on micro-calcifications concentrates enough stress around each microbody to weaken the plaque and cause rupture and thrombosis. [27, 28] The effects of repetitive ocular ductions on ONHD may be analogous.

Chronic neural tissue deformations of the magnitude described in this study have been shown to increase the risk of astrocyte activation[29] or neuropathy [20, 21]. Dynamic stretch injuries of the optic nerve in an animal model has determined that threshold strains of > 13-14% can result in histological and electrophysiological signs of injury. [30] A normal subject executes about a 150,000 saccades per day ; billions in a lifetime.[31] Repetitive motion strains have wide ranging effects on both tissue and cell functions in a variety of neural and myo-tendinous disorders.[32] Repetitive peripapillary scleral strain may also affect blood flow through the branches of the short posterior ciliary arteries that supply the ONH.[33] Additionally, mechanical stimulation of transmembrane integrin receptors, bound to the extracellular matrix of the lamina cribrosa,[34] can signal intracellular cytoskeletal structures and modulate cell structure and function.[35–39] Thus repetitive ocular ductions can in theory contribute to axonal injury.

ONHD is a slowly progressive disorder. [40–44] The prevalence of visual field defects can vary between 24-87%. [1, 45, 46] Severity of the field loss correlates with drusen size, surface visibility, [1, 46–50] mean RNFL thickness and Ganglion cell layer thickness [47, 50–52]. Visual fields may slowly and insidiously decline with age[41, 44, 53]

There appear to be two parallel pathways that mediate progressive loss of visual field and axonal attrition in ONHD. **(see** figure 7**)**. We hypothesize that the repetitive gaze-induced shearing on the ONH contributes, in part, to progressive axonal injury and vascular complications of ONHD.

The first presumably involves an ill-defined neuro-degenerative axonopathy (figure 7, blue). Sietz and Kersting were the first to propose that ONHD are the byproducts of degenerating axons. [54, 55] Spencer[4] speculated that axoplasmic flow is impaired in ONHD [56, 57] Axolemmal injury causes calcium influx and or the release of endogenous calcium.[38, 58] Ultrastructural study by Tso has demonstrated disruption of the axolemma, calcification of

intracellular and extracellular mitochondria, and the formation of corpora amylacea (also containing calcified mitochondria). He proposed that extruded mitochondria serve as nidi for progressive calcification that eventually coalesce into drusen.[559] The combination of protein deposits and mitochondrial disturbances are characteristic of a variety of neurodegenerative diseases.[4, 52]

The second pathway (figure 7, red) is a mechanical consequence of progressively enlarging intrapapillary calcifications that eventually compress and damage adjacent tissues (i.e. axons, glial cells, blood vessels).[1, 2] This study would suggest that repetitive gaze-induced shearing, a previously neglected mechanical factor, may be a contributory factor in progressive axonal injury. Distinctions in the mode and temporal pattern of stress and strain may be important because repetitive shearing is more damaging to tissues than slow compression or extension. We propose that shearing injury of axons fuels a cycle of axolemmal disruption, mitochondrial extrusion and progressive calcification that increase the size and number of ONHD.

Retinal hemorrhages have been described in 2-10% of ONHD. They consist of peripapillary subretinal and superficial nerve fiber flame hemorrhages. There have been reports associating ONHD with ischemic optic neuropathy, central retinal artery occlusion, central retinal vein occlusion and choroidal neovascular membranes.[1, 60–65] The proposed mechanisms include compressive erosion of blood vessels, ischemic venous congestion or arteriolar occlusion [1, 2, 66, 67].

This study suggests that that repetitive mechanical shearing around a druse may also damage the border tissues and blood vessels of the ONH. The “intermediate tissue of Kuhnt” and “border tissue of Jacoby” are sleeves of glial cells that provide a barrier-cushion between axons of the ONH and retinal and choroidal layers. This region also contains small branches of the posterior ciliary artery, the arterial ring of Zinn Haller and the choroid that supply the prelaminar ONH. Repetitive shearing at the margins of the BMO contiguous to a druse might cause small bleeds that dissect into the frayed margins of the peripapillary tissue planes. Repetitive traumatic shearing in this location might also stimulate the formation of peripapillary choroidal neovascular membranes

This report has the usual constraints of a retrospective study including a small sample size. There are also the inherent limitations of the OCT including shadowing and the disadvantages of 2D imaging compared to volume scans. Most importantly, structural changes do not necessarily reflect clinically significant functional effects.

The strengths and limitations of deformation tracking analysis are discussed in detail elsewhere [17–19]. Briefly, deformation tracking is more accurate in regions of high signal quality and low noise. This is important in this work, as signal quality decreases quickly with depth in an elevated optic disc. Hence, it was not possible to consistently image the lamina cribrosa. For this reason we focused our analysis of gaze induced deformations in the prelaminar region. The small deformations measured within drusen are within the accuracy expected for a region with low signal quality. The resolution of our OCT, and the use of B-

scans for analysis also prevented our tracking from measuring the deformations in the regions immediately adjacent to the drusen.

Lastly there are a number of open questions about the hypothetical model presented in figure 7 that need to be illucidated including the root cause of the axonopathy, the relative contributions of neurodegenerative versus biomechanical pathways in axonal attrition, and the long term consequences of repetitive ocular ductions in ONHD as well as other optic neuropathies.

Acknowledgments

Supported in part by: NIH EY023966 and NIH EY025011.

Abbreviations.

AION	anterior ischemic optic neuropathy
BMO	basement membrane opening
GM	geometric morphometrics
ONH	optic nerve head
ONHD	optic nerve head drusen
PC	Principle component
PCA	principle component analysis
ppBM-layer	peripapillary basement membrane layer
SDOCT	spectral domain optic coherence tomography

BIBLIOGRAPHY

1. Auw-Haedrich C, Staubach F, Witschel H. Optic disk drusen. Surv Ophthalmol 2002;47(6):515–32. [PubMed: 12504737]
2. Friedman AH, Gartner S, Modi SS. Drusen of the optic disc. A retrospective study in cadaver eyes. Br J Ophthalmol 1975;59(8):413–21. [PubMed: 1203227]
3. Friedman AH, Henkind P, Gartner S. Drusen of the optic disc. A histopathological study. Trans Ophthalmol Soc U K 1975;95(1):4–9. [PubMed: 1064209]
4. Spencer WH. XXXIV Edward Jackson Memorial Lecture: drusen of the optic disc and aberrant axoplasmic transport. Ophthalmology 1978;85(1):21–38. [PubMed: 76301]
5. Tso MO. Pathology and pathogenesis of drusen of the optic nervehead. Ophthalmology 1981;88(10):1066–80. [PubMed: 7335311]
6. Sibony PA. Gaze Evoked Deformations of the Peripapillary Retina in Papilledema and Ischemic Optic Neuropathy. Invest Ophthalmol Vis Sci 2016;57(11):4979–87. [PubMed: 27661851]
7. Chang MY, Shin A, Park J, et al. Deformation of Optic Nerve Head and Peripapillary Tissues by Horizontal Duction. Am J Ophthalmol 2017;174:85–94. [PubMed: 27751810]
8. Wang X, Beotra MR, Tun TA, et al. In Vivo 3-Dimensional Strain Mapping Confirms Large Optic Nerve Head Deformations Following Horizontal Eye Movements. Invest Ophthalmol Vis Sci 2016;57(13):5825–33. [PubMed: 27802488]

9. Malmqvist L, Bursztyn L, Costello F, et al. The Optic Disc Drusen Studies Consortium Recommendations for Diagnosis of Optic Disc Drusen Using Optical Coherence Tomography. J Neuroophthalmol 2017.
10. Sanfilippo PG, Cardini A, Hewitt AW, et al. Optic disc morphology--rethinking shape. Prog Retin Eye Res 2009;28(4):227–48. [PubMed: 19520180]
11. Adams DCR FJ; Slice DE Geometric Morphometrics: ten years of progress following the “revolution”. Italian Journal Zoology 2004;71:11.
12. Rohlf FJ. Morphometrics at SUNY Stony Brook. http://lifebiosunysbedu/morph/.
13. Zelditch M, Swiderski DL, Sheets HD. Geometric morphometrics for biologists : a primer, Second edition ed2012; x, 478 pages.
14. Sibony P, Kupersmith MJ, Rohlf FJ. Shape analysis of the peripapillary RPE layer in papilledema and ischemic optic neuropathy. Invest Ophthalmol Vis Sci 2011;52(11):7987–95. [PubMed: 21896851]
15. Sibony P, Kupersmith MJ, Honkanen R, et al. Effects of lowering cerebrospinal fluid pressure on the shape of the peripapillary retina in intracranial hypertension. Invest Ophthalmol Vis Sci 2014;55(12):8223–31. [PubMed: 25406288]
16. Sibony P, Strachovsky M, Honkanen R, Kupersmith MJ. Optical coherence tomography shape analysis of the peripapillary retinal pigment epithelium layer in presumed optic nerve sheath meningiomas. J Neuroophthalmol 2014;34(2):130–6. [PubMed: 24625774]
17. Lall P, wei J. X-ray micro-CT and DVC based analysis of strains in metallization of flexible electronics. 16th IEEE Intersociety Conference on Thermal and Thermomechanical Phenomena in Electronic Systems (ITherm) Orlando, Florida2017.
18. Tran H, Grimm J, Wang B, et al. Mapping in-vivo optic nerve head strains caused by intraocular and intracranial pressures. Proc SPIE, Optical Elastography and Tissue Biomechanics IV2017; v. IV.
19. Sigal IA, Grimm JL, Jan NJ, et al. Eye-specific IOP-induced displacements and deformations of human lamina cribrosa. Invest Ophthalmol Vis Sci 2014;55(1):1–15. [PubMed: 24334450]
20. Sigal IA, Flanagan JG, Tertinegg I, Ethier CR. Predicted extension, compression and shearing of optic nerve head tissues. Exp Eye Res 2007;85(3):312–22. [PubMed: 17624325]
21. Edwards ME, Wang SS, Good TA. Role of viscoelastic properties of differentiated SH-SY5Y human neuroblastoma cells in cyclic shear stress injury. Biotechnol Prog 2001;17(4):760–7. [PubMed: 11485440]
22. Sigal IA, Schuman JS, Ishikawa H, et al. A Problem of Proportions in OCT-Based Morphometry and a Proposed Solution. Invest Ophthalmol Vis Sci 2016;57(2):484–5. [PubMed: 26868751]
23. Demer JL. Optic nerve sheath as a novel mechanical load on the globe in ocular duction. Invest Ophthalmol Vis Sci 2016;57(4):1826–38. [PubMed: 27082297]
24. Wang X, Rumpel H, Lim WE, et al. Finite element analysis predicts large optic nerve head strains during horizontal eye movements. Invest Ophthalmol Vis Sci 2016;57(6):2452–62. [PubMed: 27149695]
25. Wang X, Fisher LK, Milea D, et al. Predictions of Optic Nerve Traction Forces and Peripapillary Tissue Stresses Following Horizontal Eye Movements. Invest Ophthalmol Vis Sci 2017;58(4):2044–53. [PubMed: 28384725]
26. Sibony P, Fourman S, Honkanen R, El Baba F. Asymptomatic peripapillary subretinal hemorrhage: a study of 10 cases. J Neuroophthalmol 2008;28(2):114–9. [PubMed: 18562843]
27. Bluestein D, Alemu Y, Avrahami I, et al. Influence of microcalcifications on vulnerable plaque mechanics using FSI modeling. J Biomech 2008;41(5):1111–8. [PubMed: 18258240]
28. Rambhia SH, Liang X, Xenos M, et al. Microcalcifications increase coronary vulnerable plaque rupture potential: a patient-based micro-CT fluid-structure interaction study. Ann Biomed Eng 2012;40(7):1443–54. [PubMed: 22234864]
29. Rogers RS, Dharsee M, Ackloo S, et al. Proteomics analyses of human optic nerve head astrocytes following biomechanical strain. Mol Cell Proteomics 2012;11(2):M111 012302.
30. Bain AC, Meaney DF. Tissue-level thresholds for axonal damage in an experimental model of central nervous system white matter injury. J Biomech Eng 2000;122(6):615–22. [PubMed: 11192383]

31. Schiller PH, Tehovnik EJ. Neural mechanisms underlying target selection with saccadic eye movements. Prog Brain Res 2005;149:157–71. [PubMed: 16226583]
32. Barr AE, Barbe MF. Pathophysiological tissue changes associated with repetitive movement: a review of the evidence. Phys Ther 2002;82(2):173–87. [PubMed: 11856068]
33. Langham ME. The temporal relation between intraocular pressure and loss of vision in chronic simple glaucoma. Glaucoma 1980;2:427–35.
34. Morrison JC. Integrins in the optic nerve head: potential roles in glaucomatous optic neuropathy (an American Ophthalmological Society thesis). Trans Am Ophthalmol Soc 2006;104:453–77. [PubMed: 17471356]
35. Kirwan RP, Crean JK, Fenerty CH, et al. Effect of cyclical mechanical stretch and exogenous transforming growth factor-beta1 on matrix metalloproteinase-2 activity in lamina cribrosa cells from the human optic nerve head. J Glaucoma 2004;13(4):327–34. [PubMed: 15226662]
36. Kirwan RP, Fenerty CH, Crean J, et al. Influence of cyclical mechanical strain on extracellular matrix gene expression in human lamina cribrosa cells in vitro. Mol Vis 2005;11:798–810. [PubMed: 16205625]
37. Kirwan RP, Wordinger RJ, Clark AF, O'Brien CJ. Differential global and extra-cellular matrix focused gene expression patterns between normal and glaucomatous human lamina cribrosa cells. Mol Vis 2009;15:76–88. [PubMed: 19145252]
38. Tan JC, Kalapesi FB, Coroneo MT. Mechanosensitivity and the eye: cells coping with the pressure. Br J Ophthalmol 2006;90(3):383–8. [PubMed: 16488967]
39. Ingber DE. Mechanobiology and diseases of mechanotransduction. Ann Med 2003;35(8):564–77. [PubMed: 14708967]
40. Malmqvist L, Hamann S. Photographic Documentation of Optic Disc Drusen Over More Than 50 Years. JAMA Ophthalmol 2017;135(3):e165470. [PubMed: 28278345]
41. Malmqvist L, Lund-Andersen H, Hamann S. Long-term evolution of superficial optic disc drusen. Acta Ophthalmol 2016.
42. Merchant KY, Su D, Park SC, et al. Enhanced depth imaging optical coherence tomography of optic nerve head drusen. Ophthalmology 2013;120(7):1409–14. [PubMed: 23531353]
43. Spencer TS, Katz BJ, Weber SW, Digre KB. Progression from anomalous optic discs to visible optic disc drusen. J Neuroophthalmol 2004;24(4):297–8. [PubMed: 15662245]
44. Lee AG, Zimmerman MB. The rate of visual field loss in optic nerve head drusen. Am J Ophthalmol 2005;139(6):1062–6. [PubMed: 15953437]
45. Mustonen E Pseudopapilloedema with and without verified optic disc drusen. A clinical analysis II: visual fields. Acta Ophthalmol (Copenh) 1983;61(6):1057–66. [PubMed: 6659908]
46. Savino PJ, Glaser JS, Rosenberg MA. A clinical analysis of pseudopapilledema. II. Visual field defects. Arch Ophthalmol 1979;97(1):71–5. [PubMed: 83136]
47. Traber GL, Weber KP, Sabah M, et al. Enhanced Depth Imaging Optical Coherence Tomography of Optic Nerve Head Drusen: A Comparison of Cases with and without Visual Field Loss. Ophthalmology 2017;124(1):66–73. [PubMed: 27817914]
48. Grippo TM, Shihadeh WA, Schargus M, et al. Optic nerve head drusen and visual field loss in normotensive and hypertensive eyes. J Glaucoma 2008;17(2):100–4. [PubMed: 18344754]
49. Wilkins JM, Pomeranz HD. Visual manifestations of visible and buried optic disc drusen. J Neuroophthalmol 2004;24(2):125–9. [PubMed: 15179065]
50. Malmqvist L, Lindberg AW, Dahl VA, et al. Quantitatively Measured Anatomic Location and Volume of Optic Disc Drusen: An Enhanced Depth Imaging Optical Coherence Tomography Study. Invest Ophthalmol Vis Sci 2017;58(5):2491–7. [PubMed: 28460051]
51. Malmqvist L, Wegener M, Sander BA, Hamann S. Peripapillary Retinal Nerve Fiber Layer Thickness Corresponds to Drusen Location and Extent of Visual Field Defects in Superficial and Buried Optic Disc Drusen. J Neuroophthalmol 2016;36(1):41–5. [PubMed: 26720518]
52. Sato T, Mrejen S, Spaide RF. Multimodal imaging of optic disc drusen. Am J Ophthalmol 2013;156(2):275–82 e1. [PubMed: 23677136]
53. Lansche RK, Rucker CW. Progression of defects in visual fields produced by hyaline bodies in optic disks. AMA Arch Ophthalmol 1957;58(1):115–21. [PubMed: 13434543]

54. Seitz R Die intraokularen Drusen [The intraocular drusen]. Klin Monbl Augenheilkd 1968;152(2):203–11. [PubMed: 4175212]
55. Seitz R, Kersting G. Der Drusen der Sehnervenpapille und des Pigmentepithels. Klin Monatsbl Augenheilkd 1962;140:75–88.
56. Jonas JB, Gusek GC, Guggenmoos-Holzmann I, Naumann GO. Optic nerve head drusen associated with abnormally small optic discs. Int Ophthalmol 1987;11(2):79–82. [PubMed: 2451648]
57. Mullie MA, Sanders MD. Scleral canal size and optic nerve head drusen. Am J Ophthalmol 1985;99(3):356–9. [PubMed: 3976813]
58. Whitmore AV, Libby RT, John SW. Glaucoma: thinking in new ways-a role for autonomous axonal self-destruction and other compartmentalised processes? Prog Retin Eye Res 2005;24(6):639–62. [PubMed: 15953750]
59. Woodford B, Tso MO. An ultrastructural study of the corpora amylacea of the optic nerve head and retina. Am J Ophthalmol 1980;90(4):492–502. [PubMed: 7424747]
60. Harris MJ, Fine SL, Owens SL. Hemorrhagic complications of optic nerve drusen. Am J Ophthalmol 1981;92(1):70–6. [PubMed: 6167172]
61. Mustonen E. Pseudopapilloedema with and without verified optic disc drusen. A clinical analysis I. Acta Ophthalmol (Copenh) 1983;61(6):1037–56. [PubMed: 6659907]
62. Rosenberg MA, Savino PJ, Glaser JS. A clinical analysis of pseudopapilledema. I. Population, laterality, acuity, refractive error, ophthalmoscopic characteristics, and coincident disease. Arch Ophthalmol 1979;97(1):65–70. [PubMed: 83135]
63. Gittinger JW Jr., Lessell S, Bondar RL. Ischemic optic neuropathy associated with optic disc drusen. J Clin Neuroophthalmol 1984;4(2):79–84. [PubMed: 6233327]
64. Rubinstein K, Ali M. Retinal complications of optic disc drusen. Br J Ophthalmol 1982;66(2):83–95. [PubMed: 7059559]
65. Hitchings RA, Corbett JJ, Winkleman J, Schatz NJ. Hemorrhages with optic nerve drusen. A differentiation from early papilledema. Arch Neurol 1976;33(10):675–7. [PubMed: 61750]
66. Brodrick JD. Drusen of the disc and retinal haemorrhages. Br J Ophthalmol 1973;57(5):299–306. [PubMed: 4123495]
67. Karel I, Otradovec J, Peleska M. Fluorescence angiography in circulatory disturbances in drusen of the optic disk. Ophthalmologica 1972;164(6):449–62. [PubMed: 4115951]
68. Ghassibi MP, Chien JL, Abumasmah RK, et al. Optic Nerve Head Drusen Prevalence and Associated Factors in Clinically Normal Subjects Measured Using Optical Coherence Tomography. Ophthalmology 2016.

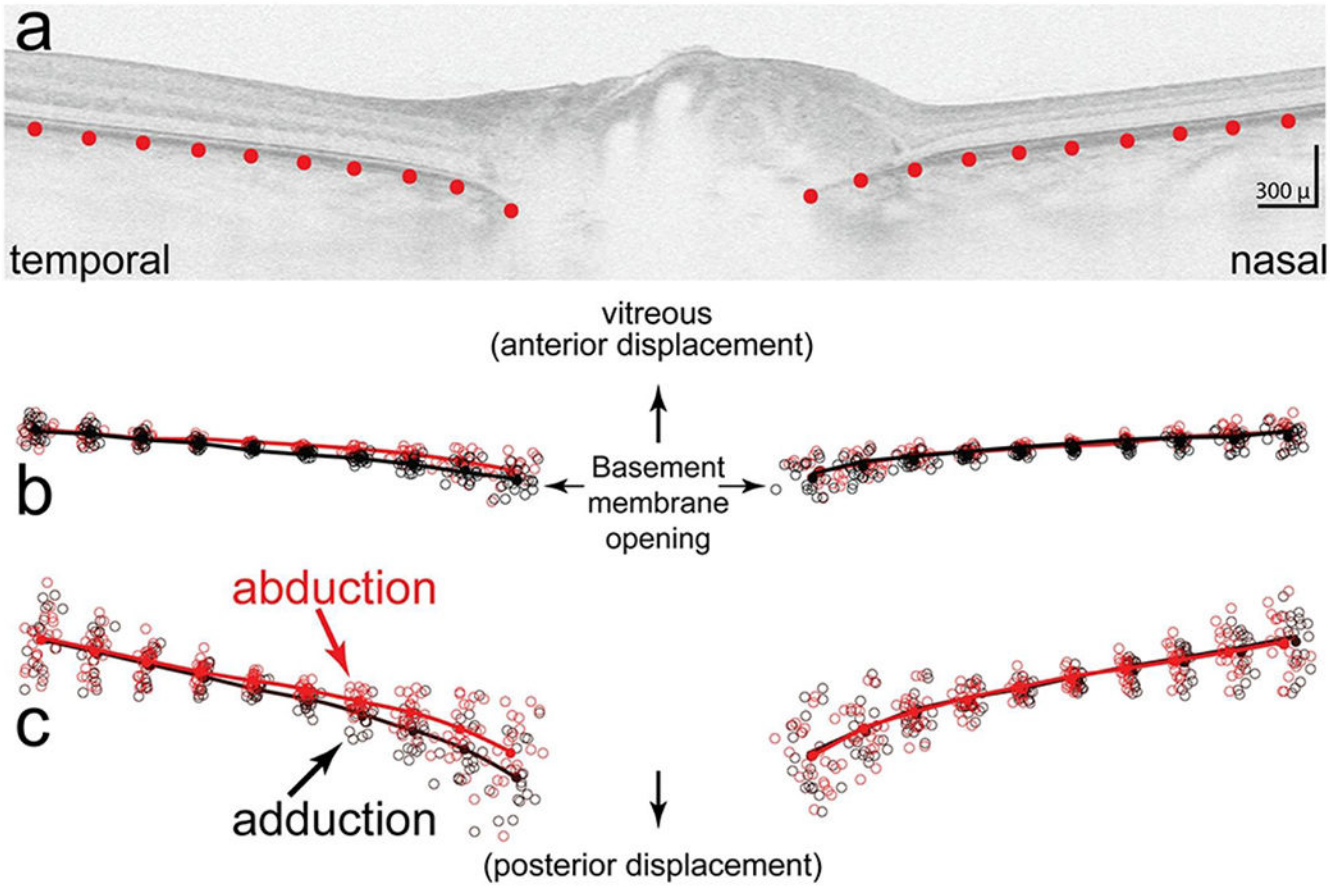

FIGURE 1.

a) Shows the placement of 10 equidistant semi-landmarks spanning 2500 µ on both sides of the basement membrane opening. b) Scatter plot that shows semi-landmarks from each subject in abduction (red circles) and adduction (black circles) after normalizing for location, size and rotation (Procrustes superimposition). The lines show the mean (consensus) shapes for each group (black for adduction, red for abduction). C. vertically stretched three fold to illustrate differences in more detail. Overall, the shape in adduction is posteriorly displaced temporally relative to the nasal side compared to abduction which is more anteriorly displaced. The difference in shapes between abduction and adduction was statistically significant ($p < 0.01$)

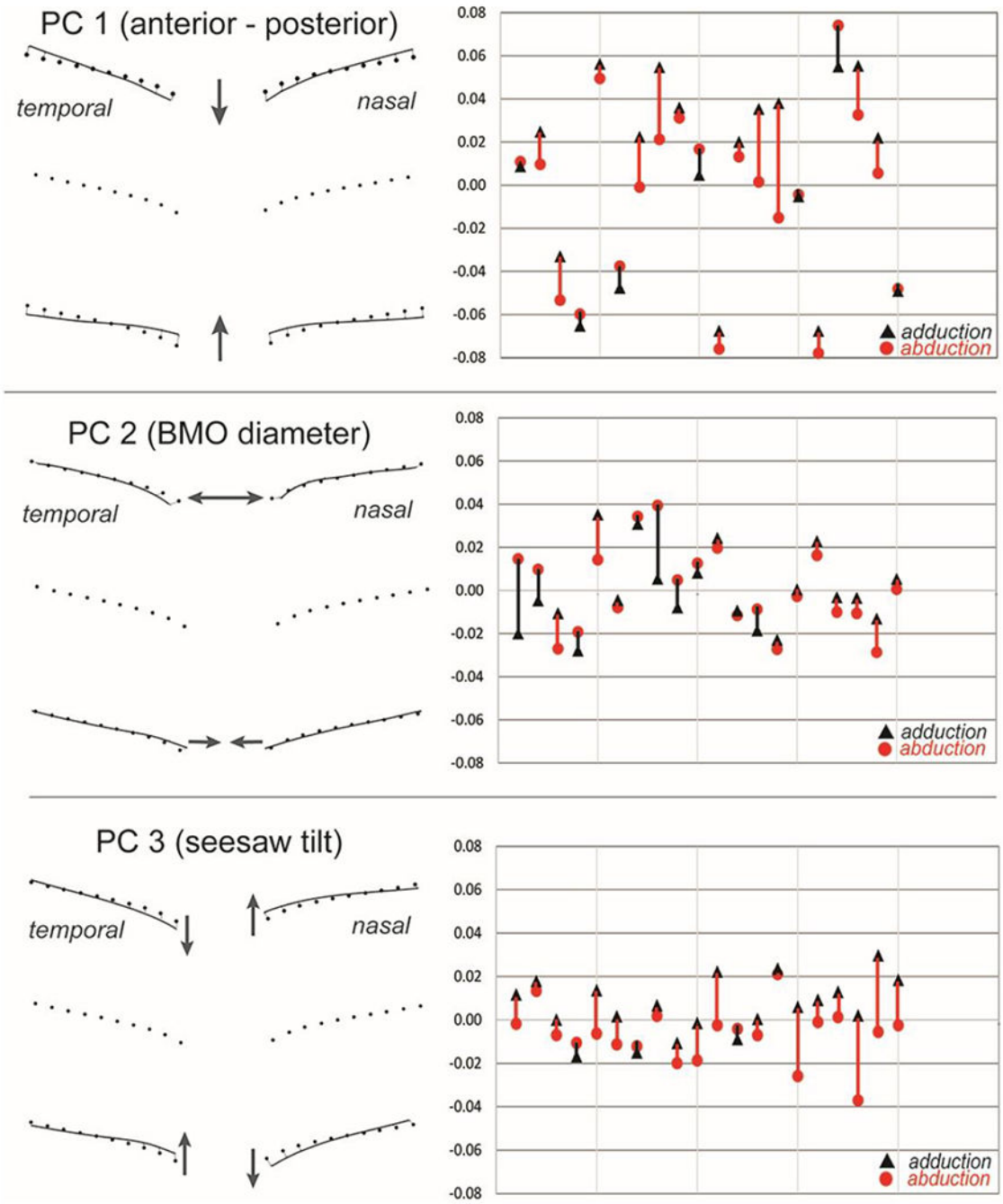

FIGURE 2.

Principal component analysis. The first three Principal components account for 90% of the variance in shape variables. A. PC1 (70%) implies a shape characterized by a symmetrical posterior (away from the vitreous, positive) to anterior (toward the vitreous, negative) deformation. B. PC2 (12%) depicts the relative diameter of the basement membrane opening and C. PC3 (8%) implies a seesaw tilting deformation. The PC scores for each patient along the abscissa represents shapes in abduction (red circles) and adduction (black triangles). A directional line connects each subject pair describing the deformation: positive shifts when

going from abduction to adduction are red, negative shifts are black. Each mark along the ordinate represents 0.100 “Procrustes distance units”.

The PC that most clearly distinguishes the shape difference between abduction and adduction is PC3. A positive shift was noted in 17 of 20 eyes. Thus, when eye position changes from abduction to adduction, the temporal side shifts posteriorly (away from the vitreous) relative to the nasal side. PC1 also shows a relative posterior displacement on adduction in 13 of the patients, although PC1 is more symmetrical than PC3. PC2 is not clearly associated with either abduction or adduction.

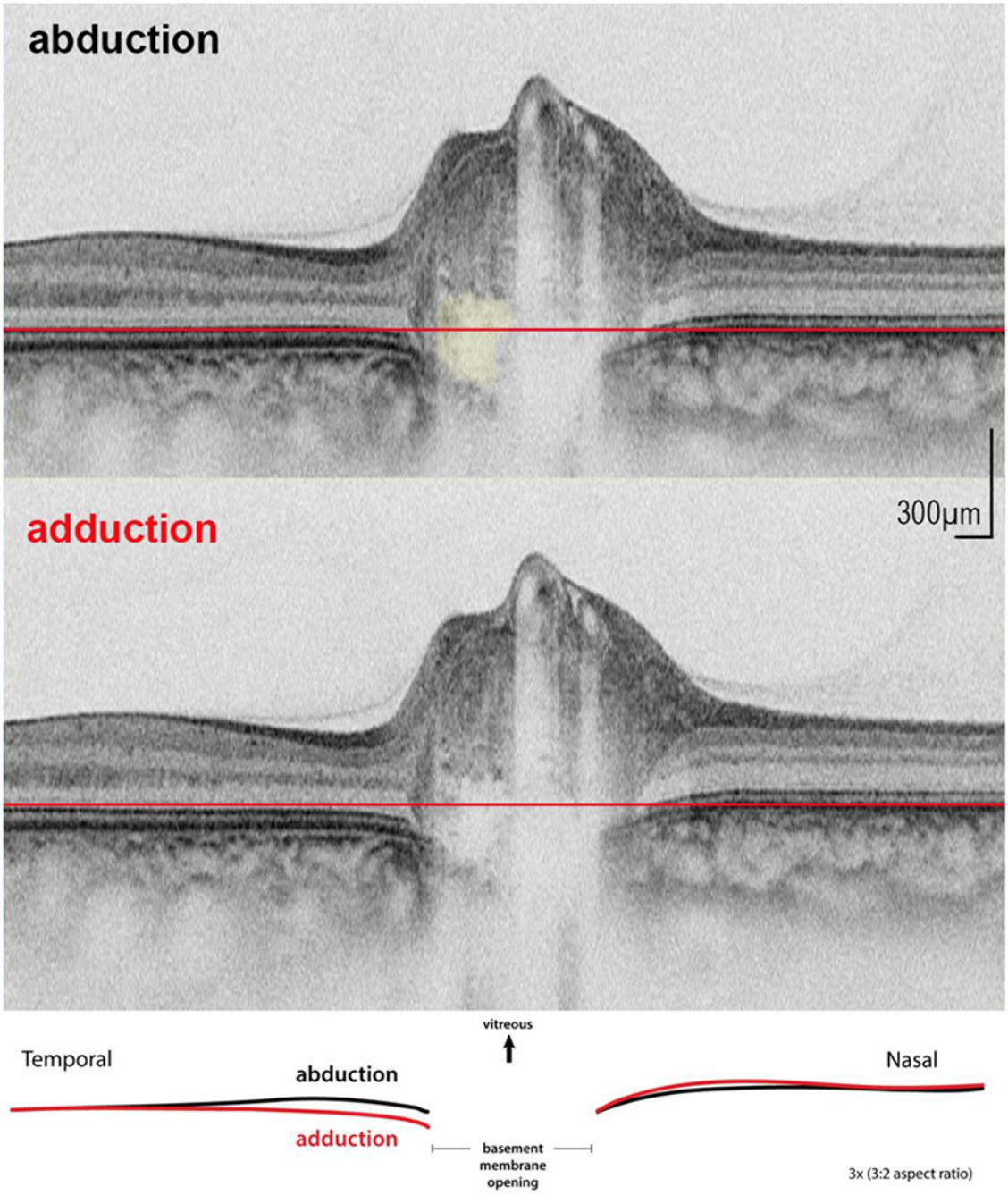

FIGURE. 3.

An example in abduction and adduction (vertically stretched image) with inset showing an overlay of the basement membrane layer from each image. Druse shown in yellow top figure. Reference plane (red line) shows that in adduction there is a small posterior displacement temporally relative to nasal side.

FIGURE 4.

Online Video clip.

Shows superimposed cyclic sequence that includes raster in primary, abduction, primary and adduction. The asterisk is located in the center of a large druse located in the basement membrane opening. There a number of hyper-reflective bands adjacent to the large druse two of which are shown with black arrows. These bands are typically seen in patients with drusen and may represent small early forms of drusen or light scattering artifact caused by drusen.[9, 68] The sequence demonstrates intrapapillary alternating seesaw deformations with posterior displacement of the BMO temporally in adduction.

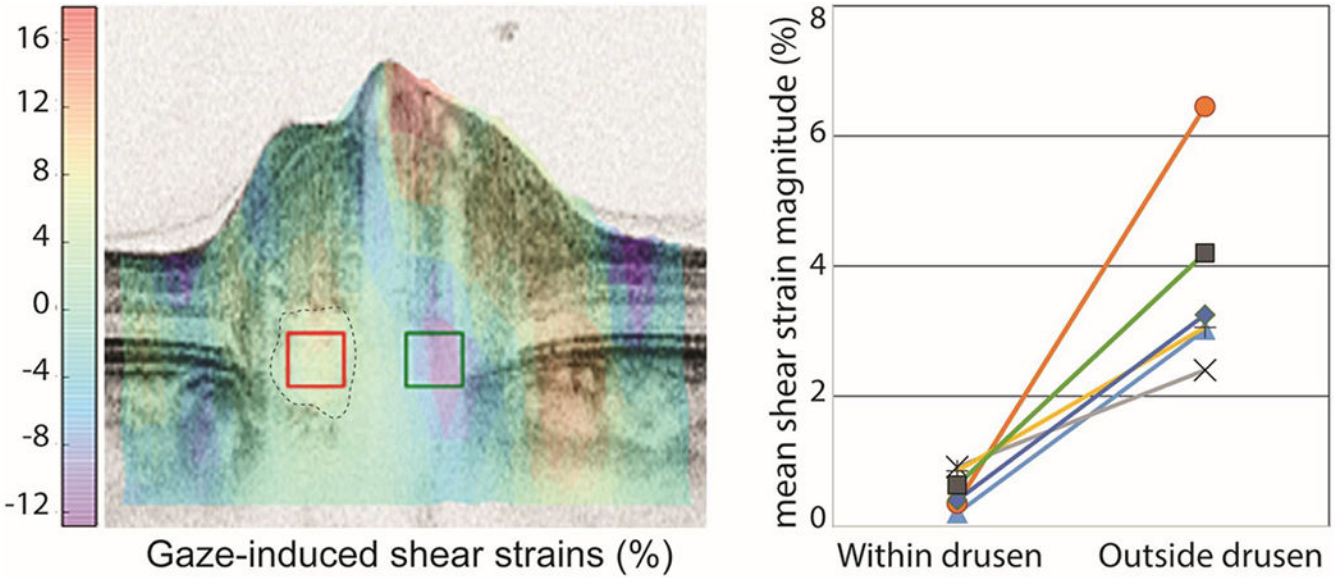

FIGURE 5.

Tracking analysis was used to compute the gaze-induced deformations from abduction to adduction. Left) B-scan of the signature case colored according to the magnitude of the shear deformation. Positive shear is clockwise, whereas negative shear is counter-clockwise. Overlaid on the colored OCT are two boxes indicating the regions where the strains within (red box) and outside (green box) the druse (dotted outline) were averaged for comparison. Note the smaller deformations within the druse than outside. The large deformations on the vessels are likely due to pulsation. Right) Change in gaze caused substantial shear strains outside the drusen but not within the drusen in all subjects ($p<0.003$, each line is a subject).

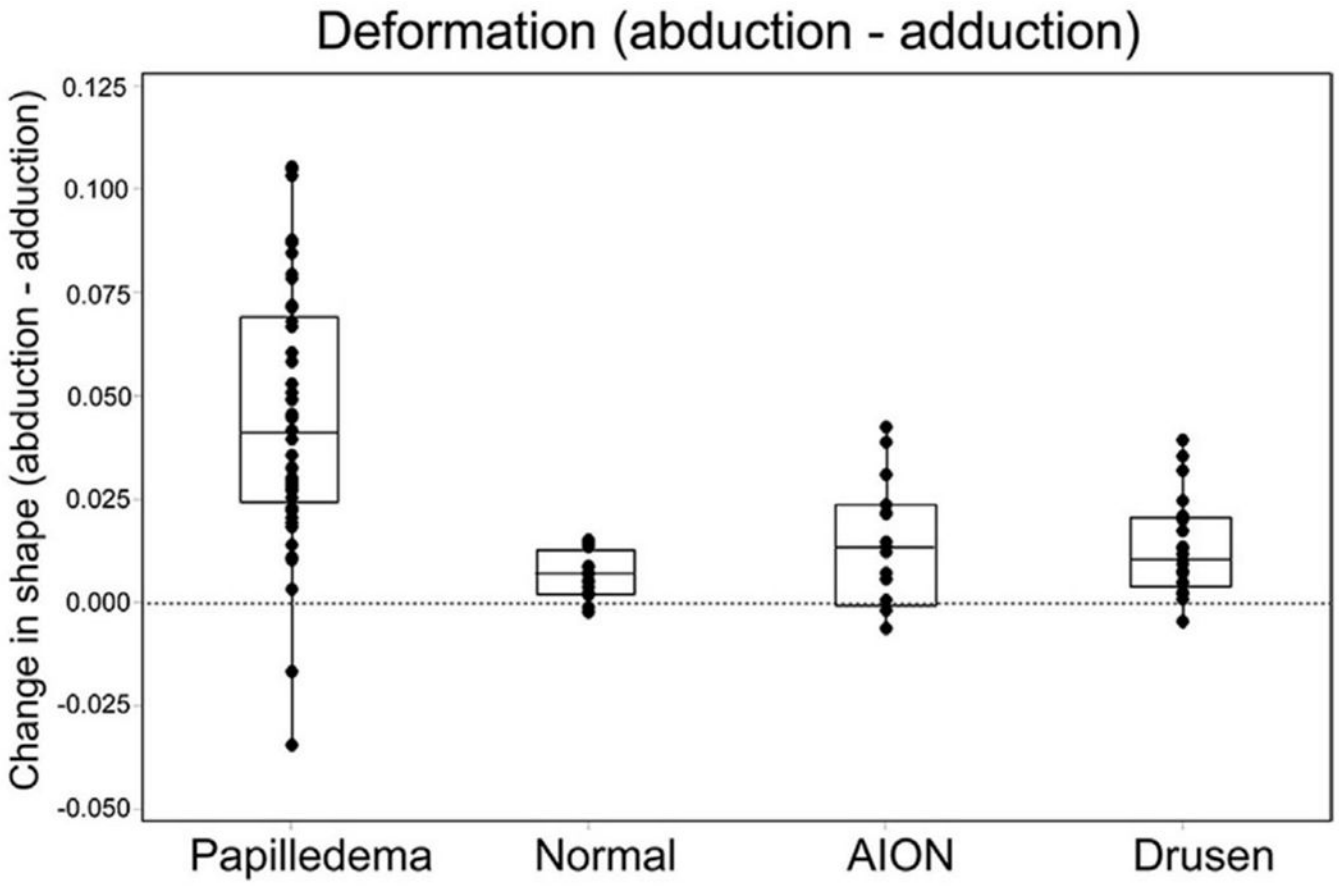

FIGURE. 6.

Each point in this plot represents the difference in shape (deformation) between abduction and adduction. Consider each point to represent the size and direction of the connecting lines between paired shapes shown in figure 2. A positive value (along the ordinate) represents a relative posterior displacement temporally / anterior displacement nasally when going from abduction to adduction; a negative value implies the reverse. Most patients showed a positive shift across all groups; however, the magnitude of these shifts varied. Deformations in normals, AION and Drusen are small compared to the large deformations in papilledema. The difference between AION, normals and drusen was not statistically different. The difference between papilledema and the other three was significant ($p < 0.001$, ANOVA). Note: data from papilledema, normal and AION has been previously published[6] but the methodologies for ONHD were identical to the other groups. This figure represents a reanalysis of the entire cohort as a group.

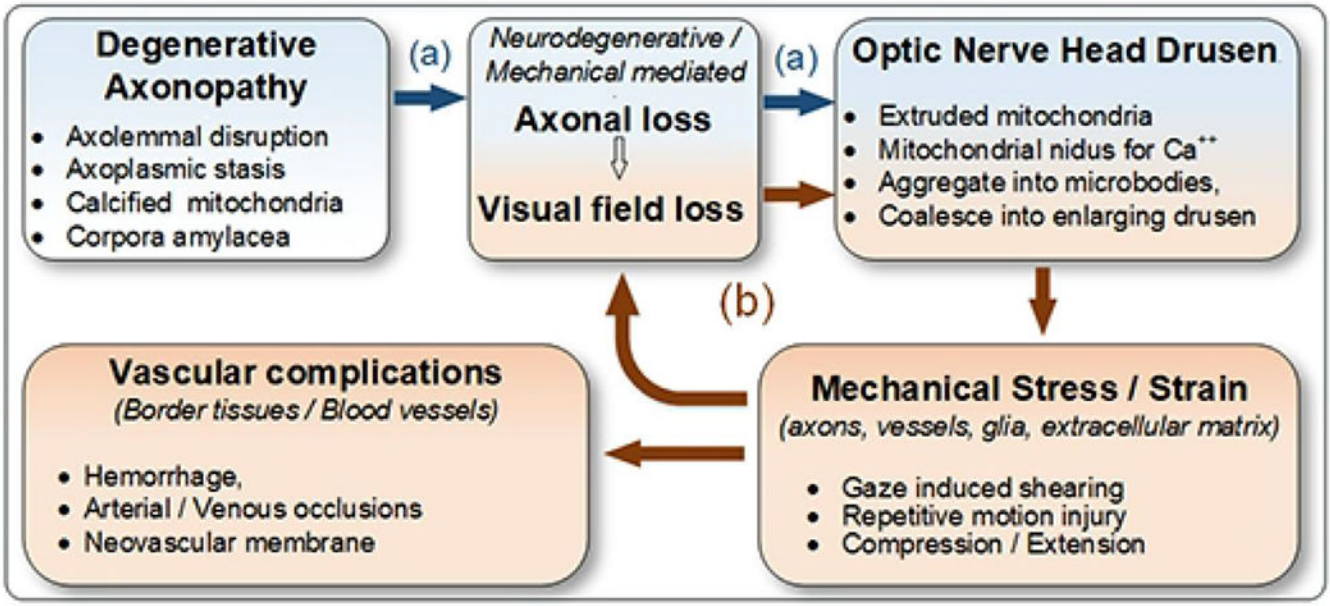

FIGURE 7.

Hypothetical pathogenesis of optic nerve head drusen formation and complications may be mediated by two parallel pathways: a. the first (blue) involves an idiopathic neurodegenerative axonopathy that presumably causes both axon loss and drusen formation; b. at some critical juncture (red), drusen enlarge enough to mechanically injure (by shearing, compression) enough axons to cause visual field defects, increase the number and the size of drusen and rarely cause a variety of vascular complications. The relative contribution of neurodegenerative and mechanical pathways to the axonal injury, progressive loss of visual fields and formation of drusen is unknown; it may vary at different points in time.